Pyrrhotite deposition through thermal projection to simulate iron sulphide slagging in oxyfuel combustion.

M.C. Mayoral*, J.M. Andrés, M.T. Izquierdo, B. Rubio
Instituto de Carboquímica, CSIC, Zaragoza (Spain)

*Corresponding autor. Address: Instituto de Carboquímica, CSIC. Miguel Luesma n.4, 50018 Zaragoza (Spain). E-mail: mayoral@icb.csic.es

Abstract

Oxyfuel combustion is envisaged as one of the main options for power production from fossil fuels in a carbon constrained scenery. There are still certain aspects of oxycombustion still on research stage, one of those is the issue of boiler materials resistance to corrosion due to solid deposits formed as a consequence of slagging in CO_2 rich flue gases. The novel approach to the issue is the simulation of realistic slagging by pyrite projection through an oxyacetylene spray gun, flying along a controlled flame and impacting onto metallic surfaces of selected composition for fireside waterwall construction (F22, P91, 409, 347, 304H and I800HT). Metallic surface temperature was kept at 400, 500, 600 and 700ºC, and after deposition, metallic coupons were aged for long periods (150 and 1500 hours) at the selected conditions (O_2/N_2, CO_2/N_2) . The characterization of deposits was performed with XRD, SEM-EDX and carburization tests.

The first finding is that the oxidation scale progression is different when partially transformed pyrite covers metallic surfaces: chromium oxide grows as a response to oxidation between the steel and the deposit, less dense and partially interrupted, and no iron oxide scale is generated. There is a clear presence of chromium sulphides in competence with the chromium oxide. On the other hand, comparison of scales in CO_2 vs. air indicates same chemical composition but different morphology: in air combustion, corrosion layers are thicker and cracked. These results can improve the prediction of operational problems in coal oxyfuel combustion.

1. Introduction

Oxy-fuel coal combustion is envisaged as a promising technology for power production from fuel sources. There is an important public and private effort in the development of demonstration plants and calculations of final economic feasibility of carbon emissions reduction after oxyfuel combustion. Despite of that, ash related problems are still a matter of concern, recognized as a mayor source of uncertainty in the technology [1]. In fact, slagging, fouling, corrosion and fuel blending continue to be the leading coal quality concerns of utility personnel in commercial plants [2]. Among all the mineral constituents of coal, pyrite is considered as the main responsible of slagging on heat transfer fireside surfaces, involving operational problems and materials wastage. The background of the problem is well-known: pyrite plays a mayor role in slagging due to the formation of low melting FeS-FeO intermediates (eutectic point at 940ºC) and the fluxing effect of FeO in aluminosilicates [3,4]. Early studies of pyrrhotite from coal pyrite [5,6] gave a multiphase thermochemistry model still in use, whereas kinetic knowledge is less satisfactory [7]. For this reason, studies about iron transformations in coal combustion combining drop tube reactors for realistic conditions and instrumental techniques for characterization can be found in recent literature [8-10]. The interest of pyrite transformation is renewed for the case of CO_2 recirculation in oxyfuel combustion [11,12]. In the present work, pyrite evolution is studied in simultaneous differential scanning calorimetry-thermogravimetry (DSC-TGA), which has been found to be very useful in describing deposition and fluxing phenomena in slagging conditions [13]. These results are compared with more realistic deposits: the new approach in this work is the use of a flame spraying gun, where pyrite particles flow inside a controlled flame at fast heating times reaching high flying speeds. In this way deposits are obtained at controlled surface temperatures and chemical composition is characterized by XRD and SEM as a function of gas temperature and composition, from air to

complete CO_2 recirculation as in oxyfuel combustion. On the other hand, the system ensures a high degree of contact between deposit and metallic surface. The chemistry of that interface can be studied in terms of oxyfuel gas composition. Examples of experimental evaluation of the fireside corrosion resistance can be found in the literature for oxycombustion [14,15], although the present work is the first one focused in iron sulphide deposits impact in waterwall corrosion.

2. Experimental

Natural pyrite from coal rejects is sieved and 100>Ø>30 is stored under inert atmosphere. Metallic materials were selected as a function to chromium content (purchased from Metal Samples Company Inc.) with complete composition shown in Table 1.

The thermobalance TA Inst. Q600 allows simultaneous thermogravimetry and calorimetry. Samples were laid onto the tared Pt pans and heat treatments consisted of a heating ramps of 50ºC.min^{-1} to the desired temperature. A constant flow of 100 ml.min^{-1} is maintained for all the purge gas studied: N_2, CO_2, and their mixtures.

The phase constitution of the iron species was investigated with XRD analysis using a Siemens D500 diffractometer set to select Cu Kα radiation. The diffraction angle scanned was 20-70º 2θ using a step size of 0.05º 2θ.

Sulphur content in samples was determined in a Carlo-Erba-1108 elemental analyzer.

For solids projection, a 5PII Sulzer Metco gun was selected, operated with hydrogen as fuel. The system comprised two Witt MM-Flex gas mixers provided of a proportional mixing valve with a control knob and percent scale, and variable flow settings. Stable flames were obtained with air or O_2/CO_2-N_2 mixtures, so the adiabatic flame temperature and flow gas composition were easily controlled. Several theoretical initial

gas compositions were given to an specific software (Gaseq) giving the adiabatic flame temperature and final flue gas composition. Once the conditions chosen, flames were ignited and real temperature was measured with a type S thermocouple along flame previous to solid projection. On the other hand, velocity of particles could be monitorised by the Accuraspray system. The Accuraspray is a in-flight particle sensor that provides information on the average in-flight velocity of particles projected through the flames [16].

Metallic coupons are displayed along flame central line at several distances, depending of selected coupon temperature, ranging from 400 to 700ºC. Temperature is measured by a type K contact thermocouple in the reverse of the coupon. Once the selected T is reached, the gun is triggered and pyrite powder flows along flame and impacts. Projection is maintained for two minutes to obtain a desired depth of deposit. Surface composition was analyzed for each sample by X-ray diffraction.

After analysis, samples were treated in a furnace for 150h and 1500h periods in a constant flow of 50 $ml.min^{-1}$ O_2/N_2 and CO_2/N_2, at 500 and 600ºC. Bare metallic coupons were aged as well at the same conditions to study both oxide development and carburization risk, and as blank experiments to establish comparison with projected metallic coupons. The composition of polished cross-section of samples was studied by means of scanning electron microscopy in a Hitachi S-3400 N microscope equipped with a Si(Li) EDX detector Röntec XFlash.

3. Results

3.1 Thermogravimetry

The decomposition of pyrite with temperature is seen by DSC in the weight change and the endothermic peak. It is shown in Figure 1 for purge gas CO_2, N_2 and a mixture 50% of both.

The endothermic decomposition of pyrite to pyrrhotite occurs between 500 and 700ºC in the same extent and temperature for both purge gases, as follows:

$$FeS_2 \rightarrow Fe_{1-x}S + \tfrac{1}{2} S_2 \quad (1)$$

As temperature increases, the melting point of each sample is reached. Pyrrhotite melts at 1080ºC in N_2 whereas the first endothermic peak onset temperature is 980ºC when CO_2 is the purge gas. New thermobalance experiments were performed, stopping the heating ramp just before the melting endothermic peaks, 1050ºC for N_2 as purge gas and 950ºC for CO_2 as purge gas. The samples obtained for both purge gas just after pyrite decomposition (750ºC) were as well obtained for analysis. Final composition of samples was determined by XRD (Figures 2a, 2b and 2c): pyrrhotite is the only specie in residue from pyrite heating in N_2, whereas the residue when heated in CO_2 denotes the presence of magnetite. It was proposed that CO_2 dissociates in CO and O_2 after heating to 500ºC, so transformation in CO_2 involved partial oxidation to magnetite, in accordance with Equation 2 [12]:

$$FeS_2 + CO_2\,(g) \rightarrow Fe_3O_4 + Fe_2O_3 + COS\,(g) + SO_2\,(g) \quad (2)$$

Although further oxidation of magnetite to hematite is described in the equation, no traces of Fe_2O_3 has been detected in the diffractograms.

A semi-quantitative analysis of the two main possible crystalline species (pyrrhotite and magnetite) was performed with the software package EVA 8.0 (Socabim Inc., Bruker AX Systems) by the Reference Intensity Ratios (RIR) method. Semi-quantitative

analysis is displayed in Table 2. Compositions calculated in this way are compared with weight change in thermogravimetry, and there is a coincidence of those values with the theoretical sulphur loss-oxygen gain calculated after the semiquant XRD values.

On the other hand, weight percentage of sulphur was obtained by elemental analysis, and results are displayed as well in Table 2. Provided that only pyrrhotite is detected by XRD in N_2 samples, it can be assumed that sulphur percentage allows iron calculation and the determination of sulphide stoichiometry. These results indicate that after pyrite decomposition, the obtained pyrrhotite goes on loosing sulphur as the temperature increases, as expected. In fact, pyrrhotite in sample N_2-750ºC fits better with JPC2 card 25-0411 ($Fe_{0.9}S$, Fe/S=0.95) and pyrrhotite in N_2-1050ºC with card 75-0601 ($Fe_{1.05}S_{0.95}$, Fe/S=1.105). This tendency of sulphur loss with temperature is not observed in the case of pyrite treated in CO_2: all the diffractograms in Figure 2b fit with JPC2 card 25-0411.

The main inference from these results is that in presence of CO_2, pyrite decomposes into pyrrhotite of low Fe/S ratio and, as temperature increases, sulphur is released and iron atoms are combined with oxygen rendering an oxysulphide, which Fe_3O_4 content increases while pyrrhotite stoichiometry is maintained. This oxysulphide forms an eutectic of low melting point, clearly seen in heat flow lines in Figure 1. In the same Figure, the heat flow line of pyrite treated in a mixture of N_2 and CO_2 is shown. There is an initial endothermic peak at 950ºC and a second one, with larger area, at 1075º, which would indicate the coexistence of an oxysulphide melt and a pyrrhotite phase with a composition similar to that obtained in pure nitrogen. In fact, XRD profiles of pyrrhotite (Figure 2c) are similar to those obtained in N_2 (Figure 2a) in terms of intensity ratios. These results have implications when applied to coal combustion: if low-NOx configuration is used, rendering pyrite decomposition in reductive gas flow, final composition would be pyrrhotite, whereas if CO_2 recirculation is installed, CO_2 rich flue gas tends to partially oxidize the iron sulphide into oxysulphide, so a decrease in

melting point should be expected in oxyfuel combustion. Prior to rising any conclusion from these results obtained by DSC-TGA, further studies about pyrite decomposition were undertaken resembling particle fast heating in a flame spray gun, which is described in next section.

3.2. Projection of pyrite over metallic coupons

Flame spraying is a typical procedure for solids projection over selected surfaces, to produce coatings and fillings of desired composition. The basis of the technique is that the solids that flow along the flame attain high temperature and melt, so they fly as fused particles that impact as splats forming a dense layer of the material. The temperature and speed reached depend on the gas mixture that feeds the gun. Among all the thermal projection systems, flame spraying is not the system of choice for heavy duty metallic or ceramic coatings, where plasma spraying of high velocity oxyfuel projection are selected, because oxygen content in plume is better controlled and higher velocities are attained, rendering better quality coatings. Nevertheless, flame spraying is more flexible in terms of feeding gas and type of solids, so for this work a 5PII Sulzer Metco gun was selected, designed to operate with acetylene or hydrogen. Oxyacetylenic flames gave very high adiabatic flame temperature, so hydrogen was selected as fuel. Table 3 gives a list of gas mixtures and adiabatic flame temperatures selected for this study. Conditions 1 and 2 were used to obtain deposits with high oxygen excess in flue gas. Conditions 3-4, and 5-6 were used to compare the different flame profiles and coupon temperature in N_2 and CO_2 for the same flame T in low oxygen excess and stoichiometric oxygen. An example of the degree of control of the system is shown in Figure 3, where profiles of flame T, coupon T and particle velocity are displayed. Flame temperatures presented a similar trend for C4-C6 conditions, as designed. Metallic targets are displayed as well along the plume axis to measure the impact surface

temperature, revealing different profiles as a function of gas composition. The control of gas flows renders particle velocities around 20m/s, which is in the range of particle velocities found in radiant zones in coal combustion [17]. This parameter is important to ensure a proper simulation of particle deformation and adherence upon impact. The convenience of this technique for solids projection is shown in Figure 4a-d. Figures 4a, 4b and 4d show the pyrrhotite deposited onto the metallic surface, and Figure 4c shows the cross section image where depth and porosity can be seen. These images indicate the satisfactory simulation of deposits formation since a dense and well adhered fused layer is obtained. Moreover, the technique allows the control of metal temperatures, which is an important parameter in slagging simulation: Figure 4d shows the external image of a deposit held at 500ºC where surface crystallised oxides are observed. Surface composition of deposits obtained by the conditions studied was analysed by XRD and phase percentages are calculated from the diffractograms, results displayed in Table 4.

The first important result is that pyrrhotite is the main specie found at 400ºC for all the conditions studied, which it is to say, at the longer distances from flame front and longer residence time. The gun is triggered for two minutes in each experiment, so it can be considered that pyrite decomposes into pyrrhotite in a flying time of 2ms, and is deposited onto a metallic surface at 400ºC. There, it is swept by a flame at a temperature given in the trends in Figure 3, which is not higher than 600ºC. When metallic coupons are held at 500ºC, pyrrhotite tends to oxidise to magnetite and hematite, in an extent which depends on the oxygen excess in product gas: oxygen excess in conditions C3 and C4 involves that half of the iron is present as oxides, mainly hematite. No significant differences can be found as a function of CO_2 presence or absence in the gas flow, comparing C3 vs. C4 and C5 vs. C6. In the case of coupons maintained at 600ºC, higher extent of oxidation is reached, although differences in flame temperature could account for that final composition.

3.3. Long treatment of bare and projected metallic coupons

Oxidation scales for all the materials were measured and depths were compared as a function of temperature and oxidation gas for furnace treatments at 500ºC and 600ºC for 150 hours in O_2/N_2 and O_2/CO_2. As expected, nickel alloys did not suffer oxidation corrosion at 500 and 600ºC treatments, and austenitic steels suffer minor surface oxidation. Ferritic steels as 409, P91 and F22 developed oxidation scales, composed of a dual layer of chromium oxides on the steel and outer iron oxides scales, thicker chromium oxide scale in the case of CO_2 oxidation. This behaviour had been previously described in oxidation studies in oxycombustion environments [18,19]. In the present work, these samples were used as blank experiments to be compared with projected samples oxidation, as it will be shown below. On the other hand, these bare oxidised samples were analysed under standard carburization characterization, because the risk of chromium carbide compromising protective oxidation should be determined. It is worth mentioning in this point that the analysis indicated no risk of carburization. Aging of steels previously projected with pyrite (transformed into monosulphide pyrrhotite along flame) at 500ºC for 150h developed different oxidation patterns (Figure 5): chromium oxide grows as a response to oxidation between the steel and the deposit, less dense and partially interrupted, and no iron scale is generated. There is a clear presence of chromium sulphides in competence with the chromium oxide. Similar results are obtained for steel 409. At 600ºC, Figure 6 shows the comparison of corrosion when aged in CO_2 versus air treatment: sulphidation points were detected in the same extent for both cases. Moreover, when the comparison is extended to 1500h (figure 7), the images show that sulphidation corrosion progress in depth, with an homogeneous distribution of sulphur in the chromium oxide corrosion scale. For those deposits with hematite composition, such as those obtained at 700ºC pyrite projection (Table 4), not

sulphidation was found at 1500h 600ºC aging periods, as expected since there was no sulphur involved in the oxidation chemistry, and the SEM images indicated the absence of surface chromium oxide nor other oxidation corrosion in the interface between the deposit and the metallic surface (Figure 8). In fact, the hematite deposit seem to behave as a protective scale to oxidation when comparing the images obtained for the same treatment in bare coupons. Those metallic coupons with higher chromium content were not affected by sulphidation.

4. Discussion

There are two different approaches to pyrite and mineral matter transformations studies: slow heating ramps, as those found in TGA or TPD-MS [12, 20-22], that ensure chemical reaction control of kinetics, and fast heating as in drop tubes, closer to pulverized coal boilers [4,5,8,9] which need to account for particle size to describe diffusional limitations. These works are extensively reviewed in [7], and have as common starting point the kinetic model for pyrite transformation in combustion environment proposed in the late 80's [23]. There, a complete decomposition of pyrite into molten pyrrhotite is described to be reached in 40ms (at the conditions selected for the calculations) and 2000ºC as possible particle maximum temperatures. In this work, thermogravimetric studies described in Section 3.1 could give the conclusion that pyrite decomposition in CO_2 atmospheres would render particles with lower melting point, implying lower viscosity which would involve higher capture rate and increased slagging. Nevertheless, the study scope is widened to rate of particle heating characteristic of that in an actual burner [24] with the use of the projection gun with the proper fuel gas mix to reduce flame temperature. But the main goal of the installation is its capability to operate with air or O_2/CO_2 mixtures, to be used in oxicombustion comparative studies. The results described in Sections 3.2. indicate that surface

composition of iron sulphide deposits is more influenced by metal temperatures than by gas composition or temperature, so no relevant differences are found when comparing oxyfuel pyritic deposits with conventional combustion ones.

On the other hand, this work basis is that highly contacted deposit layer obtained with the gun resembles more accurately real deposition than the ash replenishment methods found in the literature. The results shown in Section 3.3. indicate that the presence of iron sulphides on the tubes influences the formation of corrosive deposits by increasing the local sulphur activity in similar extent in conventional and in oxyfuel combustion. And, when the deposit is oxidized, the active fireside sulphidation corrosion mechanism is hindered, and an oxidation chromium oxide scale is not formed.

5. Conclusions

Thermogravimetric studies demonstrate that pyrite transforms into low melting point FeO-FeS in CO_2 gas and impacts onto selected metallic surfaces forming a highly contacted deposit. High gas and surface temperatures increases the degree of iron oxidation, which would imply a decrease in the extent of slagging, in the same extent for both conventional and oxycombustion. Pyrrhotite deposits involve a risk of sulphidation for low alloyed steels, being surface temperature the main parameter to describe deposit composition and its risk of corrosion: high temperature decreases the risk of sulphidation. No relevant differences were found in oxycombustion compared to conventional combustion.

Acknowledgements

The research work reported in this paper was party carried with the financial support from the RFCS contract number RFCR-CT-2006-00010 and from the Spanish Ministry of Science and Technology –FEDER with contract PN-.

References

1. Buhre BJP, Elliott LK, Sheng CD, Gupta RP, Wall TF. Oxy-fuel combustion technology for coal-fired power generation. Progr Energy Combust Sci 2005; 31:283-307.
2. Harding NS, O'Connor DC. Ash deposition impacts in the power industry. Fuel Proc Tech 2007;88:1082-1093
3. Groves SJ, Williamson J, Sanyal A. Decomposition of pyrite during pulverized coal combustion. Fuel 1987;66:461-466
4. McLennan AR, Bryant GW, Stanmore BR, Wall TF. Ash formation mechanism during pf combustion in reducing conditions. Energy Fuels 2000;14:150-159
5. Huffman GP, Huggins KH, Levasseur AA, Chow O, Srinivasachar S, Mehta AK. Investigation of the transformations of pyrite in a drop-tube furnace. Fuel 1989;68:485-490
6. Lambert JM, Simkovich G, Walker PL. Production of pyrrhotites by pyrite reduction. Fuel 1980;59:687-690
7. Hu G, Dam-Johansen K, Wedel S, Hansen JP. Decomposition and oxidation of pyrite. Progr Energy Combust Sci 2006;32:295-314
8. Zeng T, Helble JJ, Bool LE, Sarofim AF. Iron transformations during combustion of Pittsburgh no. 8 coal. Fuel 2009;88:566-572
9. Korbee R, Shah KV, Cieplik MK, Bertrand CI, Vulthaluru HB, van de Kamp WL. First line ash transformations of coal and biomass fuels during pf combustion. Energy Fuels 2010;24:897-909
10. Gupta S, Al-Omari Y, Sahajwalla V, French D. Influence of carbon structure and mineral association of coals on their combustion characteristics for pulverized coal injection (PCI) application: Metallurgic Mater Tran B. 2006;37:457-473
11. Sheng C, Li Y. Experimental study of ash formation during pulverized coal combustion in O_2/CO_2 mixtures. Fuel 2008;87:1297-
12. Bhargava SK, Garg A, Subasinghe ND. In situ high-temperature phase transformation studies on pyrite. Fuel 2009;88:988-993
13. Mayoral MC, Izquierdo MT, Andrés JM, Rubio B. Mechanism of interaction of pyrite with hematite as simulation of slagging and fireside tube wastage in coal combustion. Thermochim Acta 2002;390:103-111
14. Środa S, Mäkipää M, Cha S, Spiegel M. The effect of ash deposition on corrosion behavior of boiler steels in simulated combustion atmospheres containing carbon dioxide (CORBI PROJECT). Materials and Corrosion 2006;57:176-181
15. 1st OXYFUEL COMBUSTION CONFERENCE, 8th -11th September 2009, Cottbus, Germany. Session 2c Material Related Issues Under Oxyfuel Combustion (5 papers).
16. Bisson JF, Lamontagne M, Moreau C, Pouliot L, Blain J, Nadeau F. Ensemble in-flight particle diagnostics under thermal spray conditions. Thermal Spray 2001, NEW SURFACES FOR A NEW MILLENNIUM : International Thermal

Spray Conference (ITSC 2001), Date: MAY 28-30, 2001 SINGAPORE SINGAPORE 705-714, 2001
17. Bonin MP, Queiroz M. A parametric evaluation of particle-phase dynamics in an industrial pulverized-coal-fired boiler. Fuel 1996;75:195-205
18. Pirón Abellán J, Olszewski T, Penkalla HJ, Meier GH, Singheiser L, Quadakkers WJ. Scale formation mechanisms of martensitic steels in high CO_2/H_2O-containing gases simulating oxyfuel environments. Materials at High Temperatures 2009;26:63-72
19. Huenert D, Schulz W, Kranzmann A. Corrosion of steels in H2O-CO2 atmospheres at temperatures between 500ºC and 700ºC. ICPWS XV, Berlin, September 8-11 2008.
20. Tomeczek J, Palugniok H. Kinetics of mineral matter transformation during coal combustion. Fuel 2002;8:1251-1258
21. Yan J, Xu L, Ynag JJ. A study of the thermal decomposition of coal-derived pyrite. J Anal Appl Pyrolyisis 2008;82:229-234
22. Yani S, Zhang D. An experimental study into pyrite transformation during pyrolisis of Australian lignite samples. Fuel 2010;89:1700-1708
23. Srnivasachar S, Boni AA. A kinetic mofel for pyrite transformations in a combustion environment. Fuel 1989;68:829-836
24. ten Brink HM, Eenkhoorn S, Hamburg G. A fundamental investigation of the flame kinetics of coal pyrite. Fuel 1996;75: 945-951

Table(s)

%wt	Fe	Cr	Ni
F22	96.07	2.28	
P91	88.86	8.78	0.12
409	87.61	11.2	0.19
347	69.6	17.45	9.43
304H	71.7	18.16	8.16
I800HT	45.69	19.88	31.29
I617	1.03	21.93	54.66
I690	8.98	28.8	61.2

Table 1. Composition in weight percentage of the metallic materials selected.

		Iron specie (wt %)			Fe/S
Purge gas	TºC	pyrrhotite	magnetite	**S % wt**	ratio
N_2	750	100	0	37.95	0.936
	950	100	0	37.25	0.965
	1050	100	0	36.58	0.993
	1200	100	0	35.43	1.044
CO_2	750	91	9	34.35	
	950	80	20	30.37	
	1200	69	31	24.60	
N_2CO_2	950	98	2	36.48	
	1070	95	5	34.11	
	1200	80	20	30.35	

Table 2. XRD semiquantification and sulfur content as a function of temperature and purge gas

	Condition	1(2)	3	4	5	6
	comburent	O_2/CO_2	O_2/CO_2	Air	O_2/CO_2	Air
	oxygen	excess	excess	excess	Stoich.	Stoich.
Initial composition	N_2			0.57		0.52
	O_2	0.30	0.20	0.15	0.17	0.14
	H_2	0.33	0.37	0.27	0.38	0.33
	CO_2	0.36	0.42		0.43	
Adiab. Flame T (K)		2242	2301	2284	2249	2357
Final composition	N_2			0.66		0.61
	H_2O	0.39	0.43	0.30	0.45	0.32
	CO_2	0.42	0.48		0.47	
	CO	0.01	0.03		0.05	
	O_2	0.16	0.03	0.02	0.005	0.00

Table 3. Initial composition of the selected gas mixtures in flame spraying, and adiabatic flame temperatures and final composition calculated with Gaseq.

Coupon T	% presence XRD semiquant	C2 CO_2 (O_2 15% excess)	C3 CO_2 (O_2 3% excess	C4 Air (O_2 3% excess)	C5 CO_2 (O_2 stoi.)	C6 Air (O_2 stoi.)
400 ºC	Pirrhotite	67	87	81	84	88
	Magnetite	33	13	19	16	12
500 ºC	Pirrhotite	37	41	48	72	79
	Magnetite	25	11	17	28	21
	Hematite	38	47	35	-	-
	Flame T (ºC)		825	875	650	850
600ºC	Pirrhotite	14	22	11	38	21
	Magnetite	14	13	20	11	14
	Hematite	72	65	69	51	65
	Flame T (ºC)		1210	1125	1000	1230
700ºC	Pirrhotite				11.5	-
	Magnetite				-	-
	Hematite				88.5	100
	Flame T (ºC)				1230	1400

Table 4. XRD composition of deposits as a function of coupon temperature, and measured flame temperature at each point.

Caption of Figures.

Figure 1. Heat flow profiles in DSC of natural pyrite in N_2, CO_2 and a mixture 50%CO_2-N_2 as purge gases.

Figure 2. XRD of pyrrhotite samples obtained at different temperatures for the three purge gas studied: (a) N_2, (b) CO_2 and (c) 50%CO_2-N_2

Figure 3. Profiles of flame temperature, coupon temperature and particle velocity as a function of distance in flame axis for condition C3 and C4.

Figure 4. (a) Secondary image of deposit at 400ºC; (b) idem at x500 magnification; (c) back-scattered image of cross section of deposit at 600ºC; (d) idem surface.

Figure 5. Metallic coupon P91 aged for 150 hours, (a) aged at 500ºC, in CO_2, (b) idem, previously projected, (c) detailed magnification of (a) and elemental mapping, (d) detailed magnification of (b) and elemental mapping.

Figure 6. Metallic coupon 409 aged for 150 hours, (a) aged at 600ºC in CO_2 and elemental mapping detailed magnification, (b) aged at 600ºC in air and elemental mapping detailed magnification.

Figure 7. Metallic coupon 409 aged for 1500 hours at 600ºC in CO_2/N_2 and elemental mapping detailed magnification.

Figure 8. Metallic coupons 409 and P91 aged for 1500 hours at 600ºC in absence and in presence of deposit (projected at 700ºC).

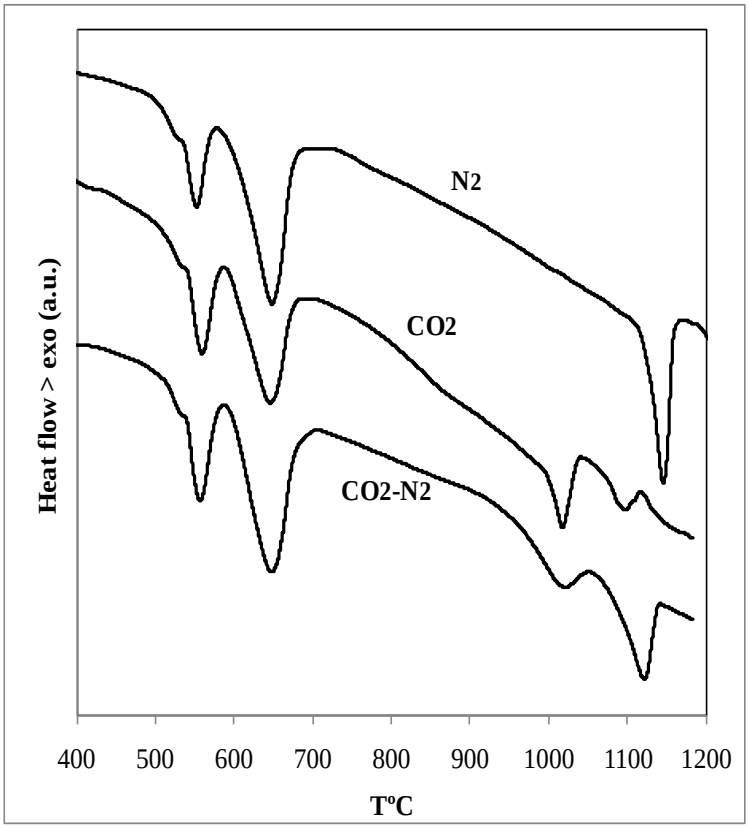

Figure 1.
Heat flow profiles in DSC of natural pyrite in N_2, CO_2 and a mixture 50%CO_2-N_2 as purge gases.

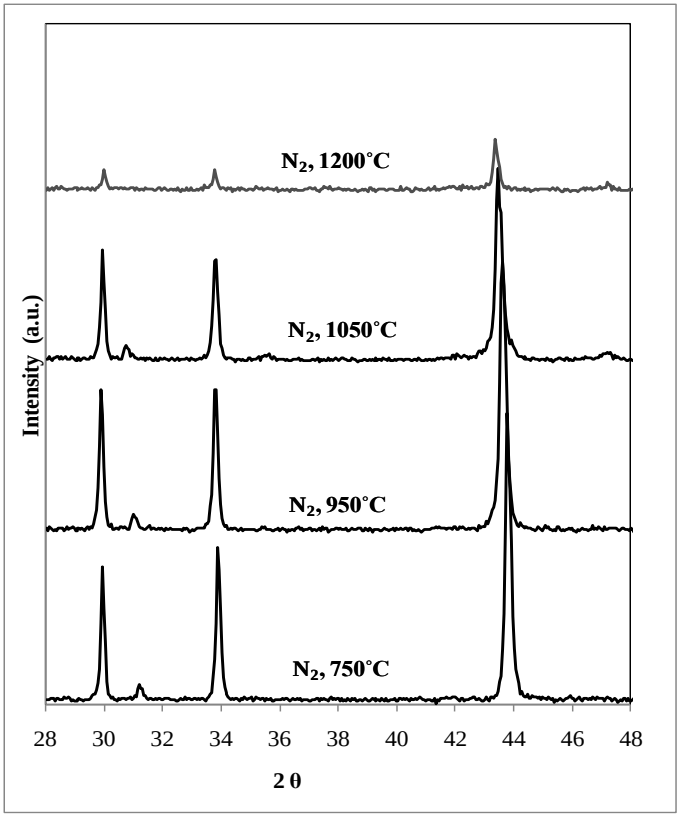

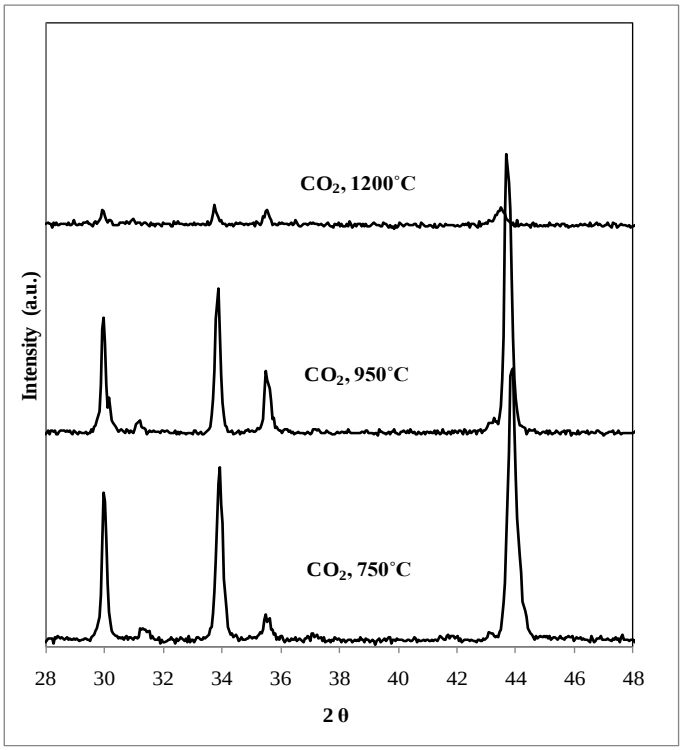

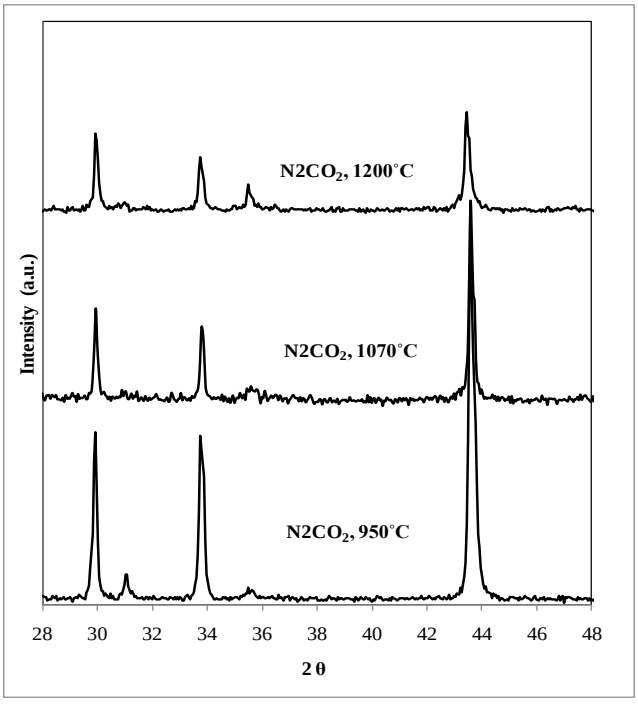

Figure 2a, 2b and 2c.

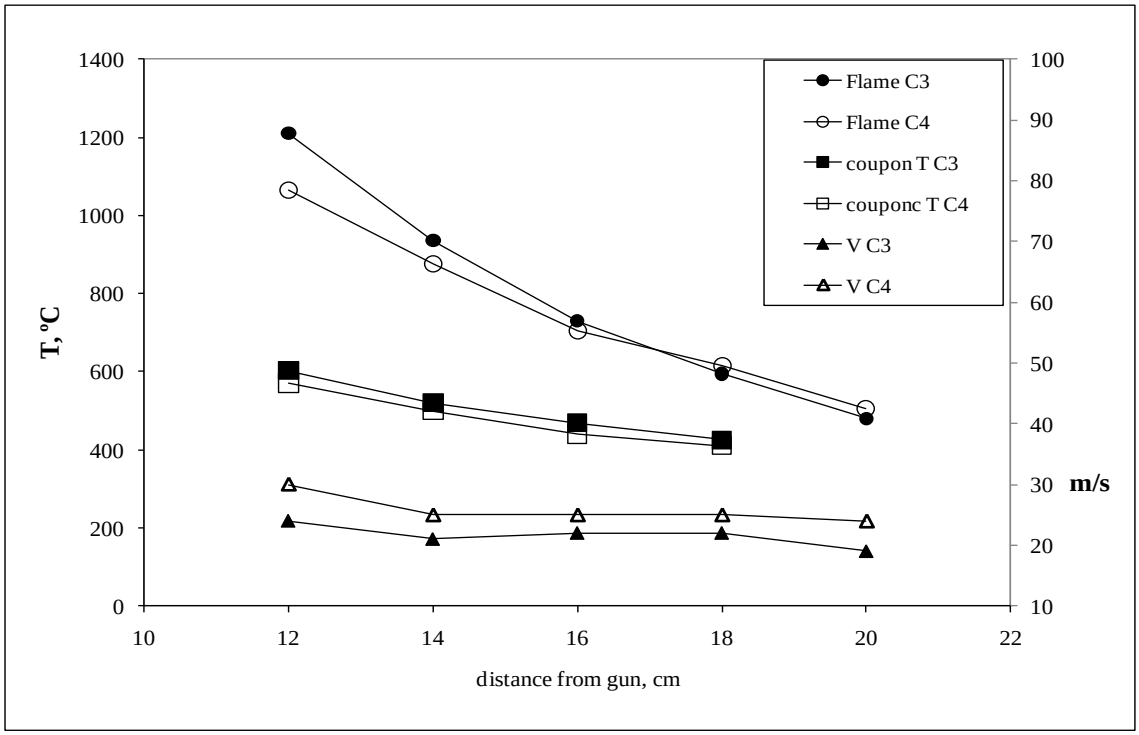

Figure 3
Profiles of flame temperature, coupon temperature and and particle velocity as a function of distance in flame axis for condition C3 and C4.

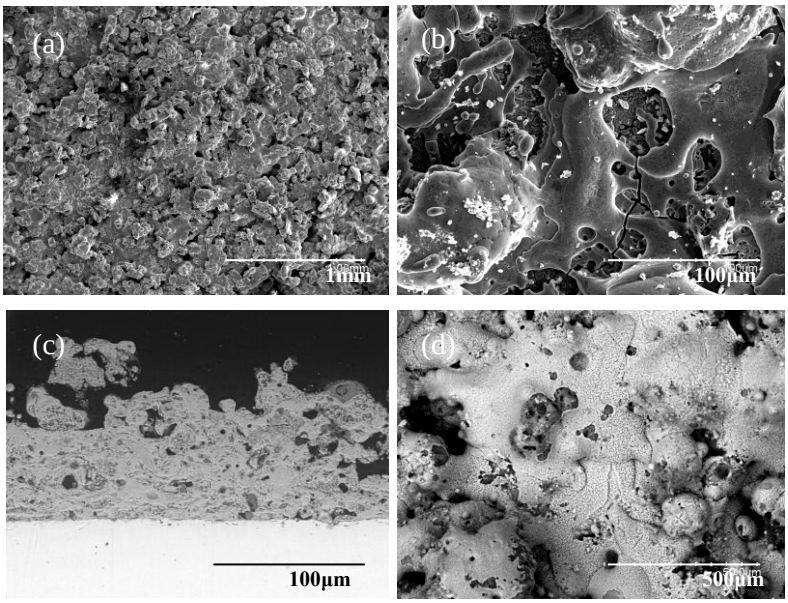

Figure 4. (a) secondary image of deposit at 400ºC; (b) idem at x500 magnification; (c) back-scattered image of cross section of deposit at 600ºC; (d) idem surface.

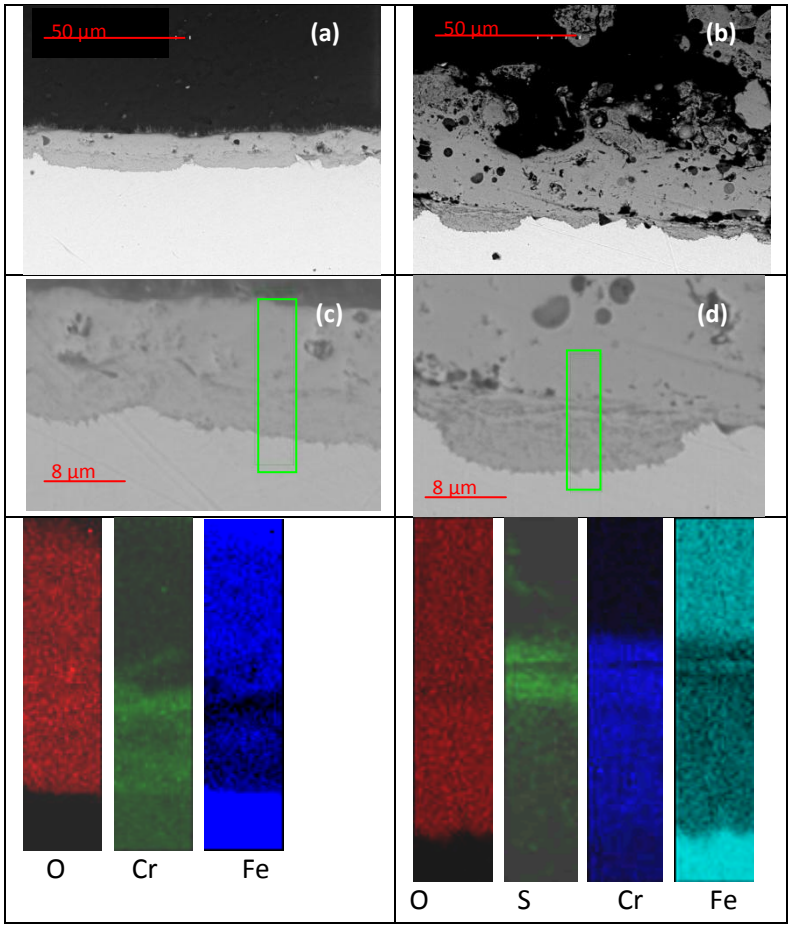

Figure 5. Metallic coupon P91 aged for 150 hours, (a) aged at 500ºC, in CO_2, (b) idem, previously projected, (c) detailed magnification of (a) and elemental mapping, (d) detailed magnification of (b) and elemental mapping.

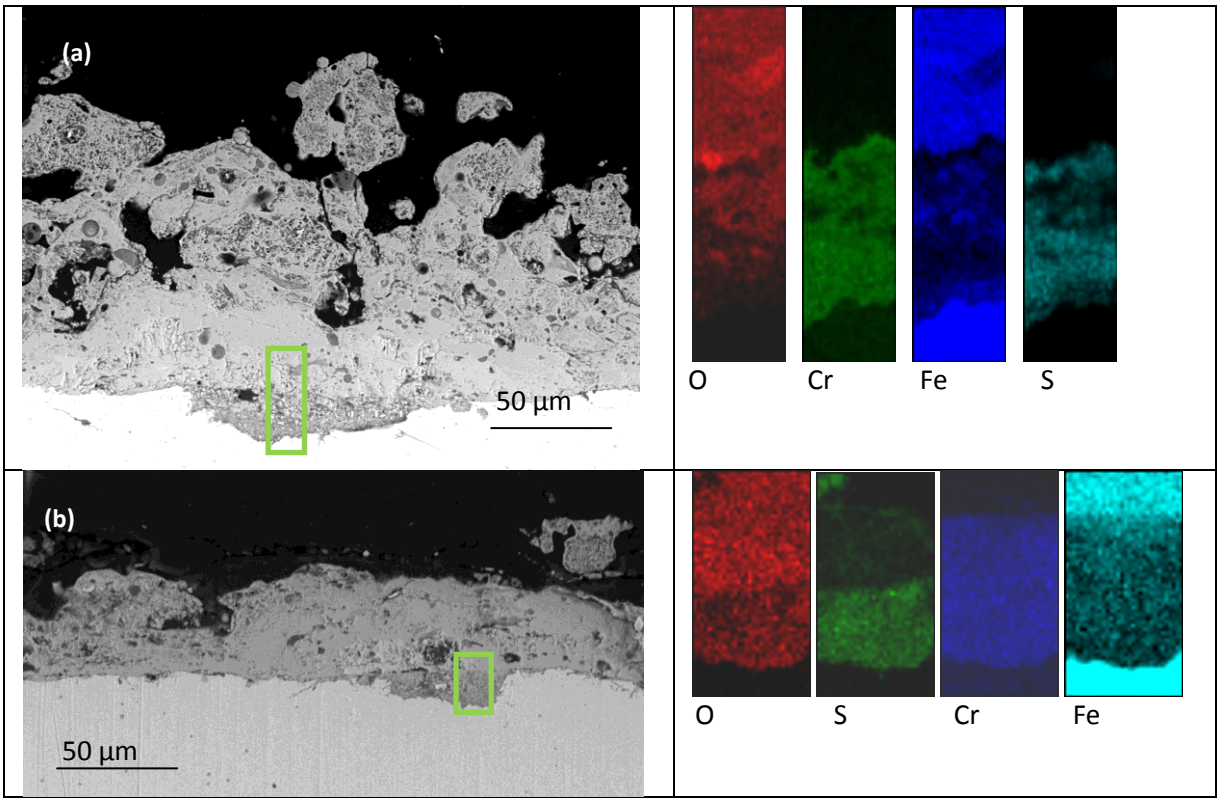

Figure 6. Metallic coupon 409 aged for 150 hours, (a) aged at 600ºC in CO_2 and elemental mapping detailed magnification, (b) aged at 600ºC in air and elemental mapping detailed magnification.

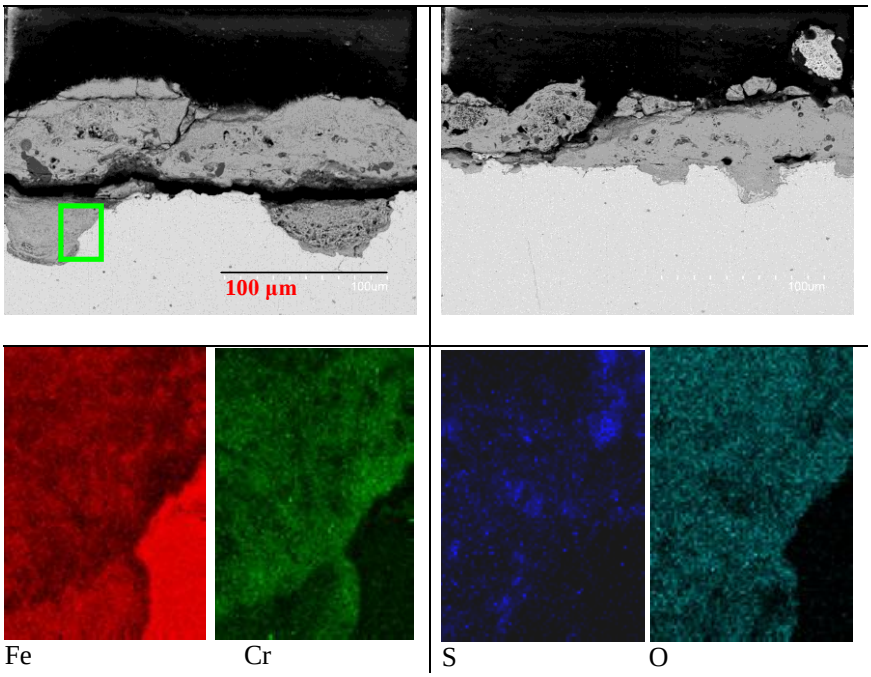

Figure 7. Metallic coupon 409 aged for 1500 hours at 600ºC in CO_2/N_2 and elemental mapping detailed magnification.

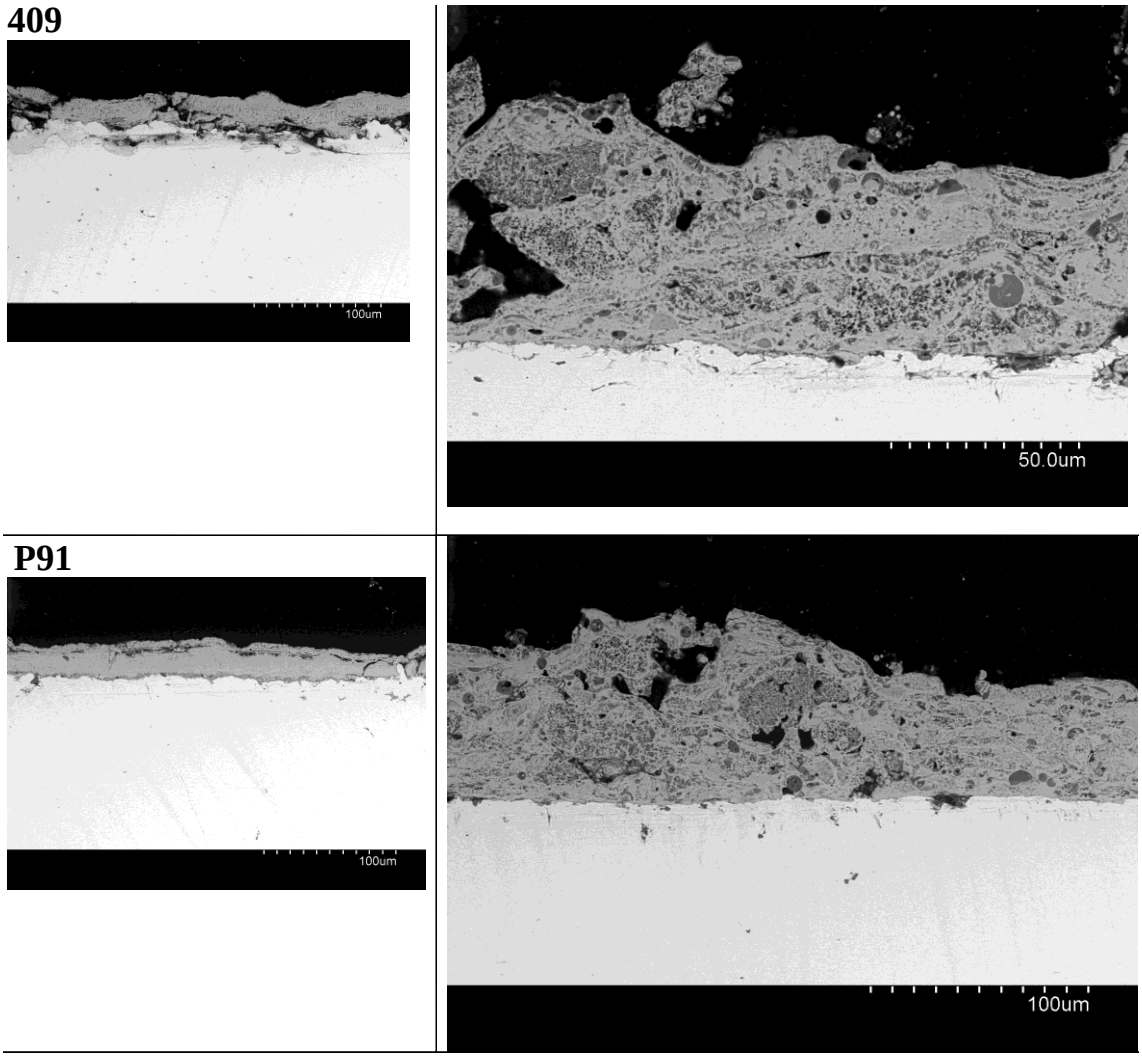

Figure 8. Metallic coupons 409 and P91 aged for 1500 hours at 600ºC in absence and in presence of deposit (projected at 700ºC)